

Switchable terahertz polarization converter based on VO_2 metamaterial

Haotian Du(杜皓天), Mingzhu Jiang(江明珠), Lizhen Zeng(曾丽珍), Longhui Zhang(张隆辉), Weilin Xu(徐卫林), Xiaowen Zhang(张小文), and Fangrong Hu(胡放荣)

Citation: Chin. Phys. B, 2022, 31 (**6**): 064210. DOI: 10.1088/1674-1056/ac4f5b
Journal homepage: http://cpb.iphy.ac.cn; http://iopscience.iop.org/cpb

What follows is a list of articles you may be interested in

Switchable instantaneous frequency measurement by optical power monitoring based on DP-QPSK modulator

Yu-Lin Zhu(朱昱琳), Bei-Lei Wu(武蓓蕾), Jing Li(李晶), Mu-Guang Wang(王目光), Shi-Ying Xiao(肖世莹), and Feng-Ping Yan(延凤平)

Chin. Phys. B, 2022, 31 (**4**): 044202. DOI: 10.1088/1674-1056/ac40ff

Wideband switchable dual-functional terahertz polarization converter based on vanadium dioxide-assisted metasurface

De-Xian Yan(严德贤), Qin-Yin Feng(封覃银), Zi-Wei Yuan(袁紫微), Miao Meng(孟淼), Xiang-Jun Li(李向军), Guo-Hua Qiu(裘国华), and Ji-Ning Li(李吉宁)

Chin. Phys. B, 2022, 31 (**1**): 014211. DOI: 10.1088/1674-1056/ac05a7

Wide color gamut switchable autostereoscopic 3D display based on directional quantum-dot backlight

Bin Xu(徐斌), Xue-Ling Li(李雪玲), Yuan-Qing Wang(王元庆)

Chin. Phys. B, 2019, 28 (**12**): 124208. DOI: 10.1088/1674-1056/ab53d1

Generation and evolution of multiple operation states in passively mode-locked thulium-doped fiber laser by using a graphene-covered-microfiber

Xiao-Fa Wang(王小发), Jun-Hong Zhang(张俊红), Xiao-Ling Peng(彭晓玲), Xue-Feng Mao(毛雪峰)

Chin. Phys. B, 2018, 27 (**8**): 084215. DOI: 10.1088/1674-1056/27/8/084215

Observation of wavelength-switchable solitons in an all-polarization-maintaining erbium-doped fiber cavity based on graphene saturable absorber reflector

Kuo Meng(孟阔), Lian-Qing Zhu(祝连庆), Fei Luo(骆飞)

Chin. Phys. B, 2017, 26 (**1**): 014205. DOI: 10.1088/1674-1056/26/1/014205

Switchable terahertz polarization converter based on VO_2 metamaterial

Haotian Du(杜皓天)[1], Mingzhu Jiang(江明珠)[1,2], Lizhen Zeng(曾丽珍)[1], Longhui Zhang(张隆辉)[1], Weilin Xu(徐卫林)[1], Xiaowen Zhang(张小文)[1], and Fangrong Hu(胡放荣)[1,†]

[1] *Guangxi Key Laboratory of Automatic Detecting Technology and Instrument, Guilin University of Electronic Technology, Guilin* 541004, *China*
[2] *Guilin Institute of Information Technology, Guilin* 541004, *China*

(Received 10 December 2021; revised manuscript received 18 January 2022; accepted manuscript online 27 January 2022)

A switchable terahertz (THz) polarization converter based on vanadium dioxide (VO_2) metamaterial is proposed. It is a 5-layer structure which containing metal split-ring-resonator (SRR), the first polyimide (PI) spacer, VO_2 film, the second PI spacer, and metal grating. It is an array structure and the period in x and y directions is 100 μm. The performance is simulated by using finite integration technology. The simulation results show that, when the VO_2 is in insulating state, the device is a transmission polarization converter. The cross-linear polarization conversion can be realized in a broadband of 0.70 THz, and the polarization conversion rate (PCR) is higher than 99%. Under thermal stimulus, the VO_2 changes from insulating state to metallic state, and the device is a reflective polarization converter. The linear-to-circular polarization conversion can be successfully realized in a broadband of 0.50 THz, and the PCR is higher than 88%.

Keywords: switchable, terahertz (THz) metamaterial, polarization conversion, vanadium dioxide (VO_2)

PACS: 42.79.Ci, 81.05.Xj, 84.30.Vn **DOI:** 10.1088/1674-1056/ac4f5b

1. Introduction

Terahertz (THz)[1] technology has become a very important scientific and technological frontier in the world. Polarization[2] is the basic property of the THz wave, because the THz waves are usually linearly polarized[3] along a specific direction. However, in the fields of THz communication,[4] imaging,[5,6] sensing,[7] and detection,[8,9] it is necessary to dynamically control the polarization state of the THz wave. The polarization converter can control the polarization state of electromagnetic (EM) waves by designing anisotropic,[10] and the traditional polarization converter is composed of polarizer[11] and wave plate,[12] which are not conducive to the integration[13] of equipment. Metamaterial[14] is an artificial material consisting of periodic sub-wavelength structures with unique EM properties, such as negative dielectric constant[15] and negative refractive index.[16] In recent years, many THz polarization converters based on metamaterial have been reported. For example, Ako *et al.*[17] demonstrated a multilayer transmission polarization converter, and its conversion efficiency is improved by using an Fabry–Perot (FP) resonator[18] composed of multilayer metal grating and H-shape resonator. Liu *et al.*[19] designed a single-layer THz metamaterial with double F-shape voids to realize cross-elliptical polarization conversion. It is noted that, the unit structures of these polarization converters are fixed after been fabricated, and the polarization state cannot be dynamically controlled.[20]

Vanadium dioxide (VO_2) is a phase transition material,[21] and its conductivity can be greatly improved under external electrical,[22,23] thermal,[24,25] and optical excitation.[26,27] Therefore, it can be used for dynamic regulation of amplitude,[28] filter,[29] and polarization.[30] In recent years, many polarization converters based on the VO_2 metamaterial have been demonstrated. Yan *et al.*[31] designed a metamaterial with broadband absorption and linear-circular polarization conversion. Using the square ring with VO_2, broadband absorption can be realized at high temperature and linear-circular polarization conversion can be realized at low temperature and a broadband. Li *et al.*[32] proposed a metamaterial with dual functions of polarization conversion and filtering. Using VO_2 strip, linear polarization conversion can be realized at low temperature. And thus, a broadband band stop filter can be realized at high temperature. However, the pattern of VO_2 in the above works is high cost and requires a variety of processes, such as magnetron sputtering, lithography, etching, coating, *etc.*

In this paper, a switchable polarization converter based on VO_2 metamaterial is designed. It consists of metal split-ring-resonator (SRR), the first polyimide (PI) spacer, VO_2 film, the second PI spacer and metal grating. At room temperature, the VO_2 is in insulating state, and the device realizes cross-linear polarization conversion. When the temperature is higher than 68 °C, the VO_2 is in metallic state, and the device realizes linear-to-circular polarization conversion. The proposed polarization converter can dynamically control the polarization of THz waves by controlling the temperature.

†Corresponding author. E-mail: hufangrong@sina.com

© 2022 Chinese Physical Society and IOP Publishing Ltd

2. Design and simulation method

As shown in Fig. 1, the designed polarization converter consists of five layers and the period in x and y directions is 100 μm. The THz wave normally incidents to the top surface of the device. The SRR on the top surface and the grating on the bottom surface are composed of aluminium, and the middle layer is VO_2 film separated by two layers of polyimide (PI), In order to obtain the best effect, the geometric parameters of the device are optimized and listed in Table 1.

Table 1. Geometric parameters of the unit cell.

t_1 (μm)	t_2 (μm)	t_3 (μm)	t_4 (μm)	t_5 (μm)	p (μm)	R (μm)	r (μm)	w_1 (μm)	w_2 (μm)	d (μm)	α (°)
0.20	59	0.20	16	0.20	100	43	37.50	5.50	5	42.50	90°

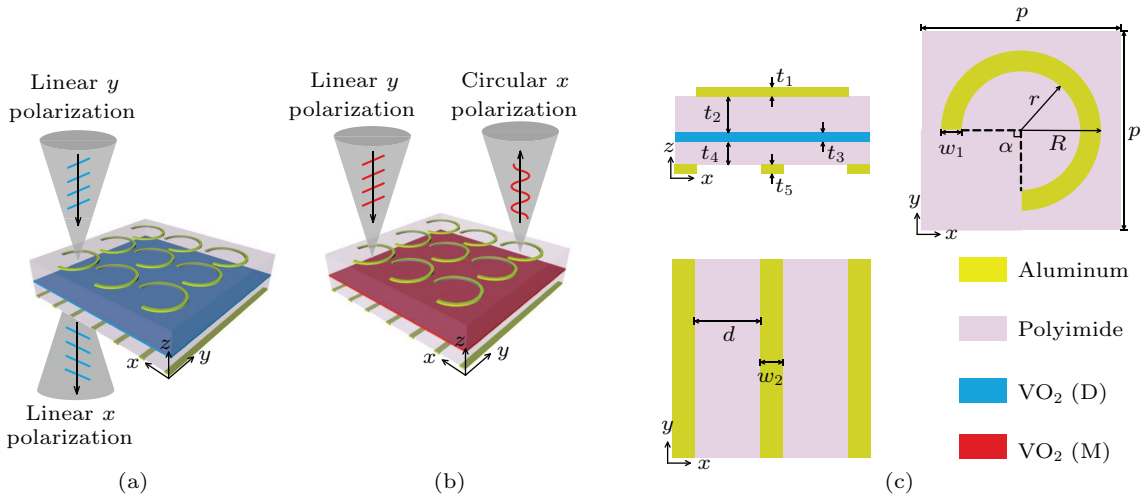


Fig. 1. Schematic diagram of the proposed polarization converter (a) for VO_2 in insulating state; (b) for VO_2 in metallic state. (c) Geometric parameters of the unit cell. VO_2 (D) and VO_2 (M) represent that VO_2 is in insulating state and metallic state respectively.

A commercialized full wave EM calculation soft CST microwave studio 2021 based on finite integration technology is used to simulate and optimize the performance of the device. The linearly y-polarized THz waves normally incident. The boundary conditions are set in the x and y directions, and open boundaries are set in the z direction. In simulation, the relative dielectric constant of PI is 3.50,[33] and the conductivity of aluminium is 4.56×10^7 S/m.[34] The Drude model[35] is used to describe the relevant dielectric constant of the VO_2 in different state,

$$\varepsilon(\omega) = \varepsilon_\infty - \frac{\omega_p^2(\sigma)}{\omega^2 + i\gamma\omega}. \tag{1}$$

The high frequency dielectric constant $\varepsilon_\infty = 12$, collision frequency $\gamma = 5.75\times10^{13}$ rad/s, respectively. The frequency of plasma ω_p is described as

$$\omega_p^2(\sigma) = \frac{\sigma}{\sigma_0}\omega_p^2(\sigma_0), \tag{2}$$

where, $\sigma_0 = 3\times10^5$ S/m, $\omega_p(\sigma_0) = 1.4\times10^{15}$ rad/s. In simulation, the σ of the VO_2 at room temperature is 3×10^2 S/m, and that for the temperature higher than 68 °C is 3×10^5 S/m, respectively.

3. Results and discussion

3.1. Switching between polarization conversion modes

At room temperature, the chemical form of the VO_2 is monoclinic crystal structure, and its physical property is insulating. Therefore, the THz waves can pass through the VO_2 film. With the increase of temperature, new chemical bonds are formed between crystals, the chemical form of the VO_2 changes to tetragonal diamond phase, and its conductivity increases. When the temperature reaches nearly 68 °C (340 K), the conductivity of the VO_2 will suddenly increase[36–38] by nearly 4–5 orders of magnitude in the range of 10 °C, and its physical property will become metallic. At this time, the THz waves will be reflected by the VO_2 film. When the temperature drops from high temperature to room temperature again, the conductivity of the VO_2 can completely returns to the insulating state.[4]

Here, we studied the influence of the VO_2 conductivity, and calculated the transmission and reflection of the device under different state of the VO_2, and the results are shown in Fig. 2. It is evident from Fig. 2(a) that the transmission decreases with the increase of the conductivity of the VO_2, while the reflection increases with it in Fig. 2(b).

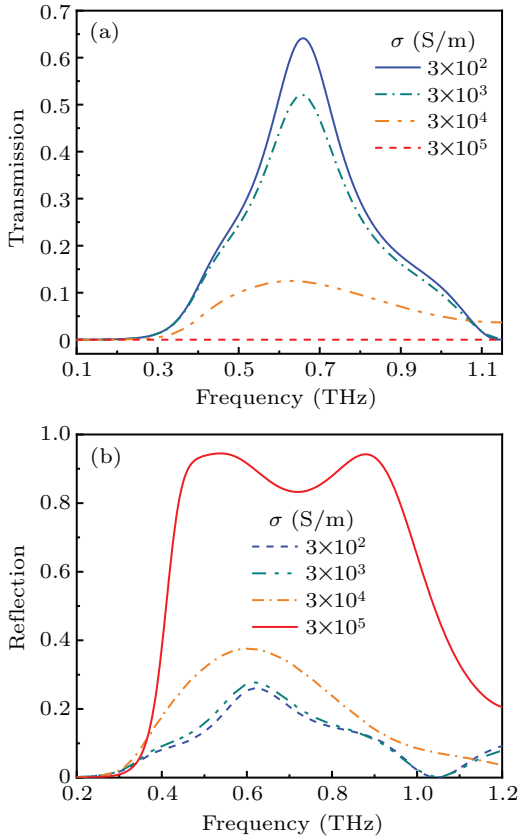


Fig. 2. (a) Transmission; (b) reflection of the device at different conductivities of the VO_2.

3.1.1. Transmission polarization conversion

When the VO_2 is at room temperature, the transmission components of t_{xx} and t_{xy} are presented in Fig. 3(a). At the central frequency of 0.66 THz, the transmission of t_{xy} is higher than 60%. The PCR can be calculated by the following formula:

$$\mathrm{PCR} = \frac{t_{xy}}{t_{xy}+t_{yy}} = \frac{|A_{xy}|^2}{|A_{xy}|^2+|A_{yy}|^2}, \tag{3}$$

where A_{xy} and A_{yy} represent the amplitudes when the incident waves are y-polarized waves, the outgoing waves are x-polarized waves and y-polarized waves, respectively.

And thus, the calculated transmission PCR is plotted as Fig. 3(b), which means that the PCR is higher than 99% in a broadband of 0.2 THz–1.0 THz. Therefore, the linearly y-polarized THz waves are almost fully converted into linearly x-polarized waves.

For further verification, the ellipticity angle (χ) is used to judge the polarization state of the THz waves. Here, the Stokes parameters S_0 and S_3 need to be introduced to calculate the χ of the THz waves, as shown below:

$$S_0 = |A^t_{xy}|^2 + |A^t_{yy}|^2, \tag{4}$$

$$S_3 = 2|A^t_{xy}||A^t_{yy}|\sin(\delta), \tag{5}$$

$$\chi = \arctan\frac{S_3}{S_0}, \tag{6}$$

where S_0 is the total intensity of the THz waves, S_3 is the circular polarization of the THz waves. A^t_{xy} represents the amplitude of the THz waves polarized in x direction after the THz waves polarized in y direction are transmitted through the sample, and A^t_{yy} represents the amplitude of the THz waves polarized in y direction after the THz waves polarized in y direction are transmitted through the sample. δ is the phase difference between the x-polarized outgoing waves and the y-polarized outgoing waves when the incident waves are y-polarized waves, $\delta = \varphi_{xy} - \varphi_{yy}$.

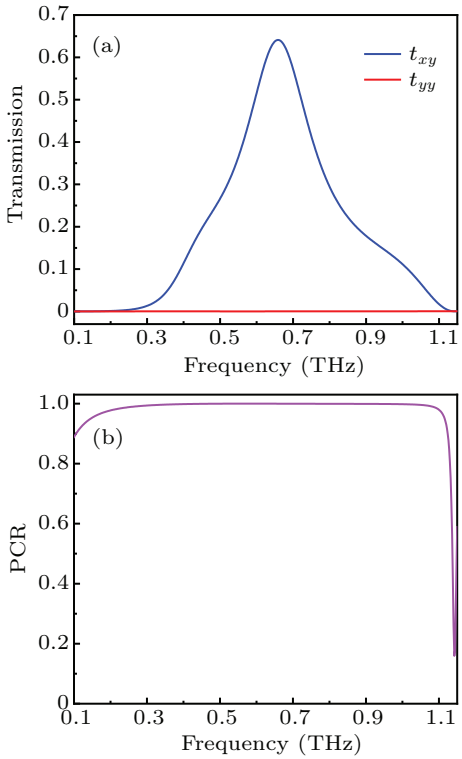


Fig. 3. (a) Transmission; (b) PCR of the device for VO_2 in insulating state.

In addition, the polarization state of the THz waves can be judged by χ, as shown in Table 2.

Table 2. Relationship between χ and polarization state.

$\chi = -\pi/4$	left-circular polarization
$-\pi/4 < \chi < 0$	left-handed polarization
$\chi = 0$	linear polarization
$0 < \chi < \pi/4$	right-handed polarization
$\chi = \pi/4$	right-circular polarization

The polarization ellipse model in electric field mode is shown in Fig. 4(a). In the electric field ellipse, S_0 represents the component of THz waves passing through or reflected by the device that are still polarized in the y direction, and S_3 represents the component of THz waves passing through or reflected by the device that are polarized in the x direction. The relationship between the values S_0 and S_3 determines the state of the polarization ellipse. In the triangle composed of semi-major axis, semiminor axis and their end connecting lines, the corresponding angle of S_3 is χ. Figure 4(b) shows that the χ of the outgoing waves is close to 0 in a broadband of 0.3 THz–1.0 THz. It means that when the VO_2 is in insulating state, the

polarization state of outgoing THz waves remains linear after transmitting through the device.

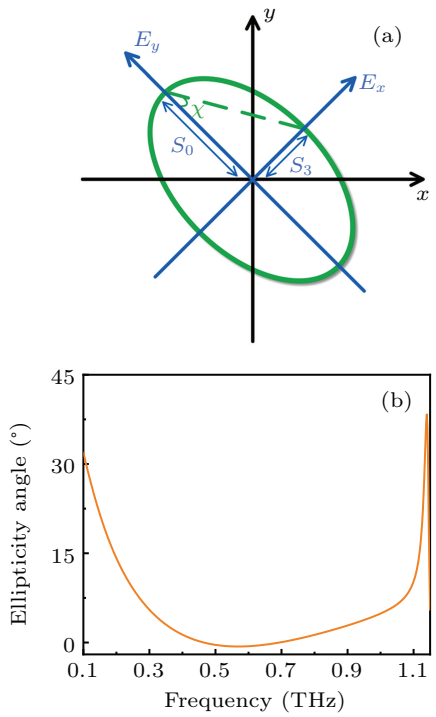


Fig. 4. (a) Polarization ellipse model in electric field mode. (b) The χ of the THz waves transmitted by the device for VO_2 in insulating state.

3.1.2. Reflective polarization conversion

When the VO_2 is in metallic state, the reflective spectra are shown in Figs. 5(a) and 5(b). They show that in a broadband of 0.44 THz–0.94 THz, the reflection is higher than 80%, and the PCR is higher than 88%, which can be calculated by formula (7). Moreover, the PCR can reach 100% in a broadband of 0.48 THz–0.55 THz and 0.86 THz–0.9 THz.

$$\mathrm{PCR} = \frac{r_{xy}}{r_{xy}+r_{yy}} = \frac{|A_{xy}|^2}{|A_{xy}|^2+|A_{yy}|^2}. \tag{7}$$

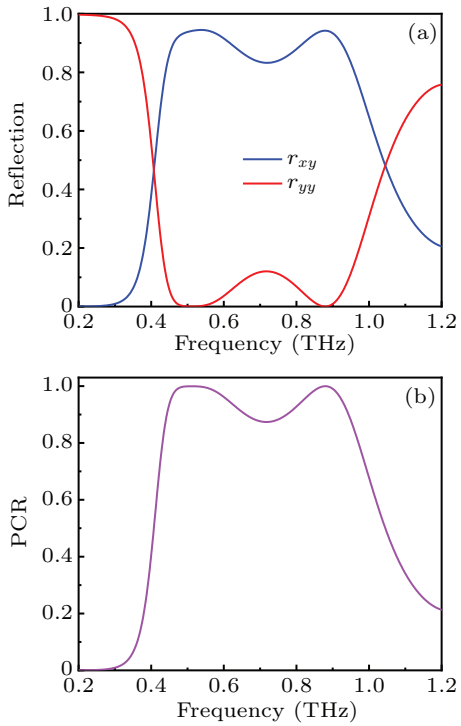


Fig. 5. (a) Reflection; (b) PCR of the device for VO_2 in metallic state.

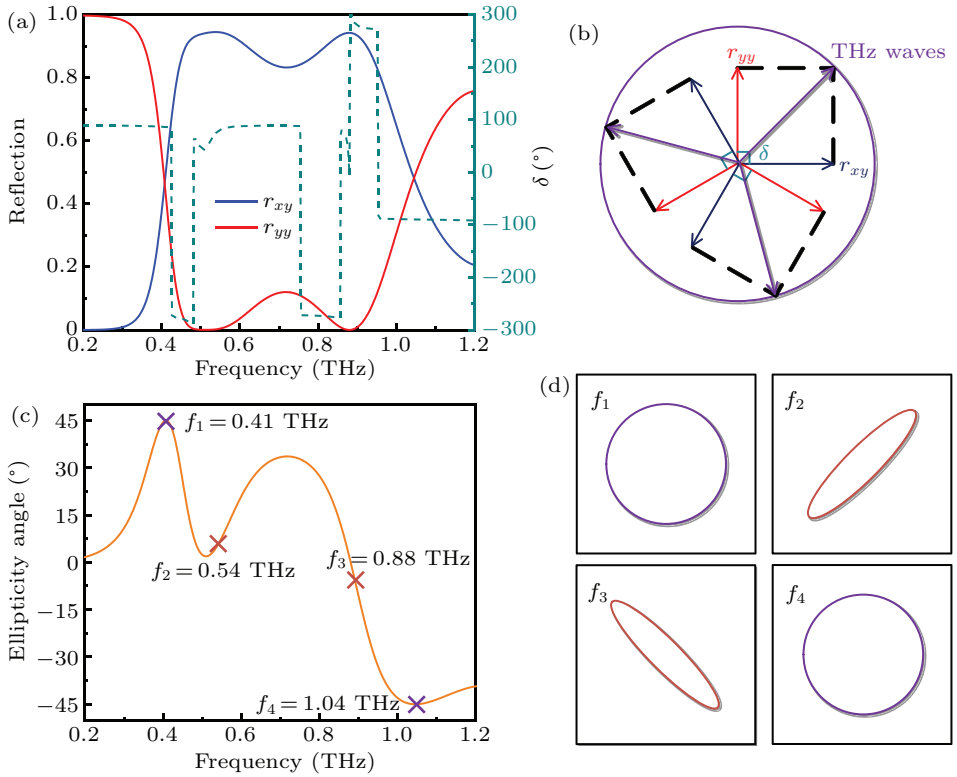


Fig. 6. (a) The δ, (b) schematic diagram of polarization conversion, (c) χ, and (d) polarization state of the THz waves reflected by the device for VO_2 in metallic state.

Figure 6(a) shows that near 0.41 THz, $r_{xy} \approx r_{yy}$, and $\delta = 90°$, indicating that the conversion of linear polarization waves to right-handed circular polarization waves is realized. Near 1.0 THz–1.1 THz, $r_{xy} \approx r_{yy}$, and $\delta = -90°$, indicating that the conversion of linear polarization waves to left-handed circular polarization waves is realized. It can be known that the polarization state of the outgoing THz waves is jointly determined by r_{xy}, r_{yy}, and δ, as shown in Fig. 6(b).

For further verification, the polarization state of outing THz waves can be determined by Table 2, as shown in Figs. 6(c) and 6(d). The polarization state at f_1 and f_4 are circular polarization state, and at f_2 and f_3 are elliptical polarization state.

3.2. Parameter optimization

In order to study the influence of different α on the performance of the device, the transmission and reflection at four different α are calculated, where α expand along the 45° direction, and the results are shown in Figs. 7(a) and 7(b), respectively. With the increase of α, the transmission spectrum shows blueshift and the transmittance decreases slightly. And there is also a blueshift in the reflection curve. Therefore, the effect is the best for $\alpha = 90°$.

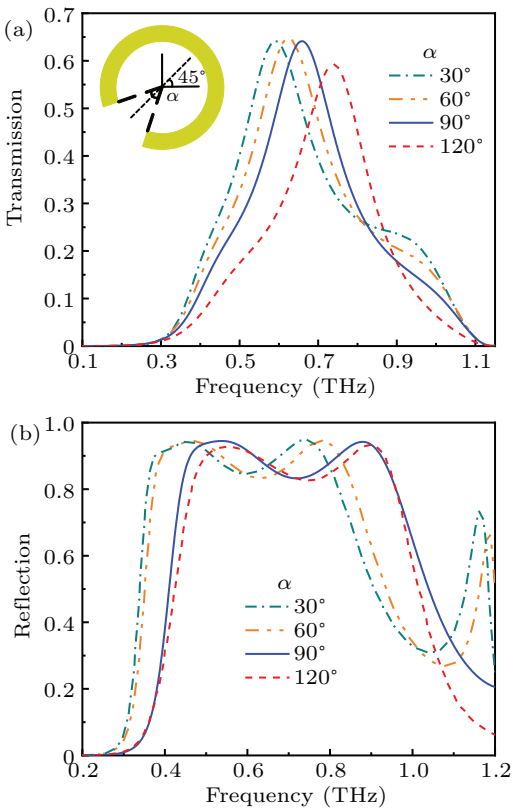


Fig. 7. (a) Transmission and (b) reflection at different α.

Moreover, the different values of the thickness of each layer (t_1, t_2, t_3, t_4, and t_5) of the device will cause the amplitude change or translation of the THz waves curve. Here, the transmission and reflection for the device with different thickness of PI are calculated, and the results are shown in Figs. 8(a) and 8(b). With the increase of thickness of PI at the down layer, the transmission decreases gradually, and it is the best at $t_4 = 16$ μm. With the increase of PI thickness at the upper layer, the reflection curve gradually changes from multiple resonant peaks to broadband, and it is the best at $t_2 = 59$ μm.

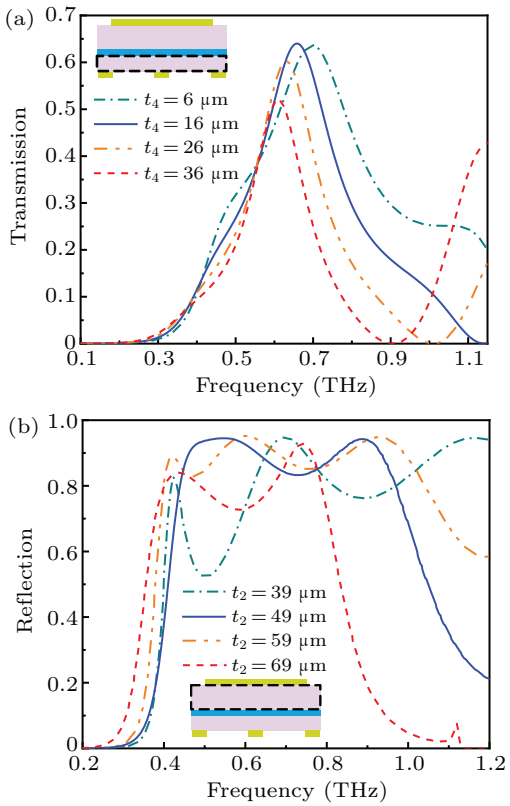


Fig. 8. (a) Transmission and (b) reflection for the device at different thicknesses of PI.

3.3. Physical mechanism

3.3.1. VO_2 is in insulating state

In order to understand the physical mechanism of the device, we calculated the distribution of surface current at different state of the VO_2. When the VO_2 is in insulating state, the surface current distribution at the resonant frequency is calculated and shown in Fig. 9(a). When the THz waves vertically incident the SRR at the upper layer of the device, the direction of the electric field is perpendicular to the propagation direction of the EM waves. At the resonance peak, the electric field excites the internal charge of the SRR ring to move along the ring and generates a ring current. The SRR can be equivalent to a magnetic dipole perpendicular to the surface of the metamaterial. And the existence of the opening destroys the original flow circuit of the charge, and the induced current will cause many heterogeneous charges to accumulate at the opening of the SRR ring and generate an electric field. The opening of the SRR is equivalent to an electric dipole, as shown in Fig. 9(b). The *LC* resonance forms on the SRR and couples

with the incident *y*-polarized THz wave. This coupling effect changes the original polarization direction of the THz wave, and the polarization conversion process begins. The resonant frequency is given by

$$f = \frac{1}{2\pi\sqrt{LC}}, \tag{8}$$

where, L is the equivalent inductance, C is the equivalent capacitance of the SRR, respectively.

As shown in Fig. 9(c), the cross-linear polarization conversion can be explained by the FP resonance of the multi-layer structure. When the linear *y*-polarized waves incident to the SRR surface, the polarization components in *x* and *y* directions will be generated by the *LC* resonance. Due to the action of the metal grating, only the polarization component in *x* direction can pass through the metal grating, while the polarization component in *y* direction is reflected to the SRR and generate the polarization components in *x* and *y* directions again. Therefore, the device can realize cross-linear polarization conversion in transmission mode.

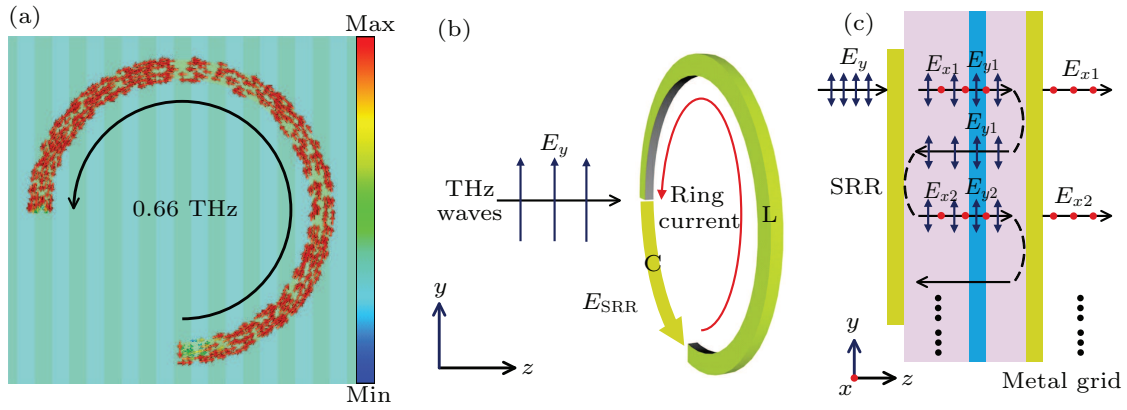


Fig. 9. (a) Surface current distribution; (b) *LC* resonance principle for VO_2 in insulating state. (c) Principle of cross-linear polarization conversion.

3.3.2. VO_2 in metallic state

When the VO_2 is in metallic state, the surface currents distribution at two resonant frequencies of 0.54 THz and 0.88 THz are calculated and presented in Figs. 10(a) and 10(b), respectively. Figure 10(a) shows that, the surface currents mainly distribute on the upper left and lower right of the SRR at 0.54 THz. At this time, the electric field is coupled with the SRR to form electric dipole resonance in *x* and *y* directions.

When the linear *y*-polarized waves incident to the SRR surface, as shown in Fig. 10(c), the polarization components in *x* and *y* directions are excited on the SRR and reflected by the VO_2 film. The polarization component in *x* direction can be first reflected on the front surface of the device, while the polarization component in *y* direction can pass through the front surface and get to the VO_2 film. And then, it can be reflected many times between the front surface and the VO_2 film with rotation of polarization. When the rotation angle of polarization reaches to 90 degrees, it can pass through the front surface again.

Figure 10(b) shows that the surface currents mainly distribute on the right side of the SRR at 0.88 THz. And thus, the electric field of the THz wave couples with the SRR, and then the electric dipole resonance forms in the *x* direction.

For the linearly *y*-polarized wave incident to the surface of SRR, as shown in Fig. 10(d), it can only generate the polarization component in *x* direction and is reflected by the VO_2 film. Therefore, the designed polarization converter can realize reflective broadband polarization conversion.

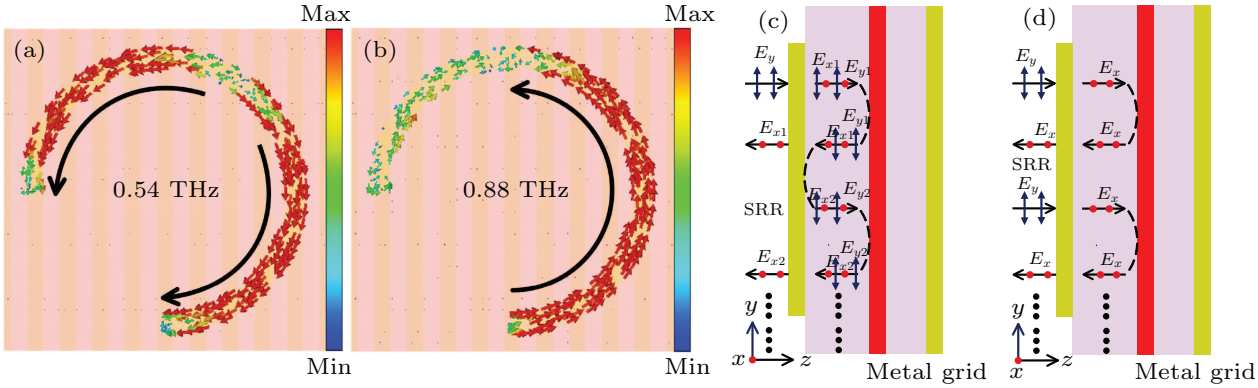


Fig. 10. Current distribution at (a) 0.54 THz and (b) 0.88 THz; broadband polarization conversion principle at (c) 0.54 THz and (d) 0.88 THz for VO_2 in metallic state.

4. Conclusion

In conclusion, a switchable polarization converter based on the VO_2 metamaterial is proposed. When the VO_2 is in insulating state, the incident THz wave produces *LC* resonance on the SRR, and then the transmitted cross-linear polarization conversion is realized by using the function of the FP cavity. When the VO_2 is in metallic state, the incident THz wave induces the electric field coupling and the FP cavity resonance between the SRR and the VO_2 films, realizing reflective broadband polarization conversion. And thus, the linear-to-circular polarization conversion in a broadband is realized. Therefore, under the thermal stimulus, the proposed polarization converter can switch freely between cross-linear polarization conversion and linear-to-circular polarization conversion.

Acknowledgements

Project supported in part by the National Natural Science Foundation of China (Grant Nos. 62065005, 61565004, 11774288, and 62003107), the Natural Science Foundation of Guangxi Zhuang Autonomous Region, China (Grant Nos. 2018GXNSFAA050043, 2020GXNSFDA238019, 2019JJB110033, and 2017GXNSFBA198029), the Innovation Project of Guangxi Graduate Education, China (Grant Nos. YCSW2021188, YCBZ2021071, and 2020YCXB04), the Foundation from Guangxi Key Laboratory of Automatic Detecting Technology and Instrument (Grant No. YQ21101); and the Research and Development Project in Hunan Province, China (Grant No. 2020SK2111).

References

[1] Nagatsuma and Tadao 2011 *IEICE Electron Express* **8** 1127
[2] Wang D and Liu J 2012 *Phys. Rev. A* **86** 023833
[3] Fan R H, Zhou Y and Ren X P 2014 *Adv. Mater.* **27** 1201
[4] Grebenchukov A, Zaitsev A and Masyukov M 2019 *J. Phys.: Conf. Ser.* **8** 012062
[5] Zhang L L, Zhong H and Chao D 2011 *Opt. Commun.* **283** 4993
[6] Wang X K, Cui Y and Sun W F 2020 *J. Opt. Soc. Am. A* **27** 2387
[7] Zhang Z Y, Fan F and Li T F 2020 *Chin. Phys. B* **29** 078707
[8] Zhang J 2014 *Opt. Lett.* **39** 4096
[9] Wang R, Han J and Liu J 2011 *Opt. Lett.* **45** 3506
[10] Wang T J and Chen Y C 2012 *Opt. Express* **20** 601
[11] Dincer F, Karaaslan M and Unal E 2015 *Mod. Phys. Lett.* **29** 334
[12] Oh M, Hwang W and King J 1997 *ETRI J.* **18** 287
[13] Ran Y Z, Shi L H and Wang J B 2019 *Opt. Commun.* **451** 124
[14] Chen X and Fan W H 2015 *Mater. Res. Express* **2** 055801
[15] Zhang K L, Hou Z L and Kong L B 2017 *Chin. Phys. Lett.* **34** 097701
[16] Zhang S, Park Y S and Li J 2009 *Phys. Rev. Lett.* **102** 023901
[17] Ako R T, Lee W and Atakaramians S 2020 *APL Photon.* **5** 046101
[18] Rakhmanov M, Savage R and Reitze D 2002 *Phys. Lett.* **305** 239
[19] Liu W W, Chen S Q and Li Z C 2015 *Opt. Lett.* **40** 3185
[20] Yahiaoui R, Guillet J P and Mounaix 2013 *Opt. Lett.* **38** 4988
[21] Nandja S and Hache A 2019 *Opt. Commun.* **449** 63
[22] Jiang M Z, Hu F R and Zhang L H 2021 *J. Lightwave Technol.* **39** 3488
[23] Zhao S, Hu F R and Xu X L 2019 *Chin. Phys. B* **28** 054203
[24] Singh D, Mittal P and Gosvami N N 2019 *Adv. Eng. Mater.* **21** 1900616
[25] Shi R, Shen N and Wang J W 2019 *Appl. Phys. Rev.* **6** 011312
[26] Parra J, Ivanova T and Menghini M 2021 *J. Lightwave Technol.* **39** 2888
[27] Pouyan S M, Miri M and Sheikhi M H 2021 *Appl. Opt.* **60** 1083
[28] Zhu F H, Du H L and Li Jiang 2018 *Appl. Phys. Lett.* **112** 081103
[29] Li T, Luo X Q and Hu F R 2021 *J. Phys. D: Appl. Phys.* **54** 435105
[30] Ren Y, Tang B 2021 *J. Lightwave Technol.* **39** 5864
[31] Yan D X, Meng M and Li J S 2020 *Opt. Express* **28** 29843
[32] Li Z W and Li J S 2021 *Appl. Opt.* **60** 2450
[33] Liu Y C, Qian Y X and Hu F R 2020 *Results in Physics* **19** 103384
[34] Liu W W and Song Z Y 2021 *Carbon* **174** 617
[35] Cocker T L, Baillie D and Buruma M 2017 *Phys. Rev. B* **96** 205439
[36] Morin F J 1959 *Phys. Rev. Lett.* **3** 34
[37] Victor J L, Gaudon M and Salvatori G 2021 *J. Phys. Chem. Lett.* **12** 7792
[38] Jiang M Z, Hu F R and Zhang L H 2021 *J. Lightwave Technol.* **39** 3488
[39] Hilton D J, Prasankumar R P and Fourmaux 2007 *Phys. Rev. Lett.* **99** 226401